Hindawi
Advances in Materials Science and Engineering
Volume 2022, Article ID 4120287, 15 pages
https://doi.org/10.1155/2022/4120287

Research Article

Damage Evolution of Rocks Containing a Set of Cross-Joints Based on Acoustic Emission Characteristics

Xiao Li,[1,2,3] **Xinquan Wang**,[1,2,3] **Kangyu Wang**,[4] **Hongguo Diao**,[1,2,3] **and He Zhang**[5]

[1]*Department of Civil Engineering Zhejiang University City College, Hangzhou 310015, China*
[2]*Key Laboratory of Safe Construction and Intelligent Maintenance for Urban Shield Tunnels of Zhejiang Province, Hangzhou 310015, China*
[3]*Zhejiang Engineering Research Center of Intelligent Urban Infrastructure, Hangzhou 310015, China*
[4]*School of Civil Engineering, Zhejiang University of Technology, Hangzhou 310015, China*
[5]*College Civil Engineering & Architecture, Zhejiang University, Hangzhou 310015, China*

Correspondence should be addressed to Hongguo Diao; diaohg@zucc.edu.cn

Received 10 August 2022; Revised 19 September 2022; Accepted 22 September 2022; Published 30 September 2022

Academic Editor: Depeng Ma

Copyright © 2022 Xiao Li et al. This is an open access article distributed under the Creative Commons Attribution License, which permits unrestricted use, distribution, and reproduction in any medium, provided the original work is properly cited.

The problem of damage rupture of jointed rocks is a hot topic of research in underground tunnel engineering. In this paper, the damage evolution characteristics of rocks containing a set of cross-joints are investigated based on particle flow code (PFC). Firstly, the jointed rock models, such as rock models with different joint cross-angles and with different joint lengths, are established based on PFC. Then, the uniaxial compression mechanical properties and acoustic emission (AE) evolution characteristics of different jointed rocks are analyzed. Finally, the damage evolution characteristics of jointed rocks are discussed based on the damage variable defined by AE counts. The research results show that the uniaxial compressive strength (UCS) and elastic modulus (E) of the jointed rock are highest when the joint cross-angle β is 60°. The UCS and E of jointed rocks show a trend of decrease with the increase of joint length. The overall trend of the AE evolution of jointed rocks does not change with the change of joint cross-angle and joint length. However, the time step of the occurrence of acoustic emission (crack initiation time) has changed. The damage evolution of jointed rocks shows three stages with the increase of stress (time): damage-free stage, slow damage increase stage, and sharp damage increase stage. The fluctuation characteristics of the damage evolution of jointed rocks are different with the change of β and LB. The damage rupture of jointed rocks begins to sprout from and expand along the tip of the joints.

1. Introduction

With the continuous increase of underground mining scale and depth, there are a number of disasters such as rock burst of roadway-surrounding rocks and instability of coal pillars. The occurrence of dynamic disasters in underground mining is related to the mechanical properties of surrounding rocks of roadways. Generally, there are a large number of defects such as joints and fractures in the surrounding rock of the roadway, which make the mechanical properties of the surrounding rock of the roadway vary greatly, leading to more difficult prevention and control of mine disasters [1–3]. Therefore, it is of great engineering significance to investigate the physical and mechanical properties of different defective rocks [4–6].

At present, the methods to study the mechanical properties and instability mechanisms of jointed rocks mainly focus on indoor experiments and numerical simulations. In terms of experimental studies, many scholars have used different materials (e.g., natural rocks, cement mortar, gypsum, and PMMA (poly(methyl methacrylate))) to explore the damage mechanical properties and characteristics of jointed rock masses with various joint characteristics [7]. For example, Lee and Jeon [8] experimentally investigated the mechanical properties of granite, PMMA, and gypsum specimens containing a noncrossing nonparallel joint under

uniaxial compression conditions. Yin et al. [9] studied the coalescence mechanism between two parallel three-dimensional (3D) preexisting surface cracks in the granite specimen under uniaxial compression. The bridge angles between the two preexisting cracks vary from 0° to 135°. Yang [10] investigated the crack coalescence behavior of brittle sandstone samples containing two coplanar fissures in the process of deformation. Zhou et al. [11] experimentally studied the crack coalescence behavior in rock-like materials containing multiple flaws under uniaxial compression. Compared with indoor experiments, numerical simulations are convenient and low cost in simulating mechanical properties and damage characteristics of different jointed rocks. At the same time, some complex joint experiments are produced with relatively large errors, and numerical simulation can ensure sufficient accuracy. Based on the finite element method (FEM) or discrete element method (DEM), Li and Wong [12], Zhang and Wong [13], and Chen et al. [14] have investigated the influence of inclination angle and loading condition on crack initiation and propagation. Vergara et al. [15] discussed the effect of joint geometrical parameters on the mechanical behavior of specimens containing nonpersistent joints using the UDEC. Sarfarazi et al. [16] studied the failure behavior of "H"-shaped nonpersistent cracks under uniaxial load using particle flow code (PFC), and the angles of "H"-shaped nonpersistent joints were 0°, 30°, 60°, and 90° degrees. Although many scholars have conducted a lot of research studies on the mechanical properties and crack extension forms of jointed rocks, the forms of engineering joints are complex and diverse, and there are still areas that need to be studied, such as the cross-angles of joints and the length of joints.

In addition, many studies have shown that the destruction process of rocks is accompanied by acoustic emission phenomenon, and the use of this phenomenon can effectively predict and analyze rock burst, envelope collapse, and other hazards [17–19]. Therefore, the acoustic emission phenomenon during the destruction of rocks with different joints is also a research hotspot for scholars. At present, many scholars have investigated the acoustic emission characteristics during rock destruction. For example, Moradian et al. [17] evaluated the damage during shear tests of rock joints using acoustic emissions. Hazzard and Young [18] provided a technique for recording AEs in bonded-particle models and applied the technique to a simulated compressive failure test on a model of granite core sample. Khazaei et al. [19] quantified the damage characteristics of intact rock based on acoustic emission technology. Lin et al. [20] experimentally studied the acoustic emission characteristics of jointed rock mass by a double disc cutter. Chong et al. [21] investigated the scale effect and anisotropy of jointed rock mass (JRM) from the perspective of acoustic emission characteristics and estimated the size of the representative element volume (REV). Zhang et al. [22] comparatively studied the fracture characteristics of coal and rock samples based on acoustic emission technology. Chen et al. [14] discussed the acoustic emission evolution characteristics of rocks with different joint dip angles under uniaxial conditions. Liu et al. [23] investigated the AE evolution characteristics and damage constitutive model of coal-rock combined body based on particle flow code. Zhang et al. [24] analyzed the effects of different joint positions on the mechanical properties, acoustic emission characteristics, and damage evolution characteristics of rock columns based on PFC models. Although many scholars have verified the relationship between rock damage and acoustic emission, studies on the acoustic emission damage evolution characteristics of jointed rocks are relatively insufficient, and there is still a need to further investigate the damage evolution characteristics of different jointed rocks.

In this paper, the damage evolution characteristics of rocks containing a set of cross-joints are investigated based on particle flow code. Firstly, the jointed rock models, such as rock models with different joint cross-angles and with different joint lengths, are established based on the parallel bond model (PBM) and the smooth joint model (SJM). Then, the uniaxial compression mechanical properties and acoustic emission evolution characteristics of different jointed rocks are analyzed. Finally, the damage evolution characteristics of jointed rocks are discussed based on acoustic emission counts.

2. Rock Models with a Set of Cross-Joints Based on Particle Flow Code

2.1. PFC Theory for Simulating Jointed Rock Mass. The particle flow code program simulates the motion of the rock medium and its interactions through the discrete particle approach. Compared with finite element and other discrete element software, the PFC has the following advantages: the basic unit of PFC is particles, and the collection of inter-particle adhesion fracture can simulate the macroscopic rock breakage; the contact between particles is better than that between angular objects, which greatly improves its computational efficiency [25].

The PFC reflects the macromechanical properties of the model by setting particles and the contact between particles. When simulating the medium (e.g., rock mass and soil), the PFC provides two contact models: the contact bond model (CBM) and the parallel bond model (PBM) [26]. Since the CBM is a point contact, it can only simulate force transfer and not moments, which in turn is only suitable for simulating materials such as soils. The PBM regards the bonding between particles as a set of parallel springs, which has the effects of tension, shear, and moment, so it can effectively simulate the bonding between particles in rocks. In this paper, we use the PBM to build the complete rock model. When the tensile or shear stress between the particles exceeds the parallel bond strength, the parallel bond will lose its function [27].

The smooth joint model (SJM) is usually used to simulate the joints and fractures in rocks in the PFC model [28, 29]. Simulation of jointed rocks was achieved by replacing the PB contact model in the PBM with the SJ contact model. As shown in Figure 1, the smooth joint model provides the macroscopic behavior of a linear elastic and either bonded or frictional interface with dilation [26]. The behavior of the bonded interface is linear elastic until the strength limit is

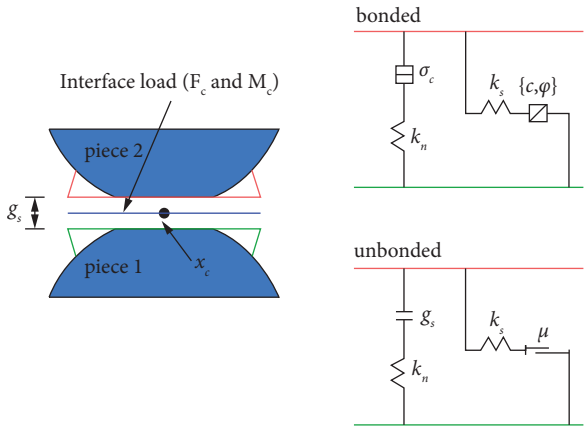

Figure 1: Smooth joint model [22].

exceeded and the bond breaks, making the interface unbonded; the behavior of an unbonded interface is linear elastic and frictional with dilation, with slip accommodated by imposing a Coulomb limit on the shear force. The interface does not resist relative rotation.

2.2. Numerical Models

2.2.1. Numerical Schemes. The purpose of this paper is to investigate the damage evolution characteristics of rocks containing a set of cross-joints, and the main considerations are the effects of the cross-angle and the length of joints, so the two schemes, as shown in Figure 2, are mainly considered in this paper. The model dimensions of the two schemes are the same, both are 50 mm × 100 mm, and both fixed the inclination angle (30° with the horizontal line) and the length LA (20 mm) of joint A. In Figure 2(a), the length LB of joint B is fixed as 30 mm, but its angle β with joint A is varied. The joint cross-angle β is taken as 30°, 60°, 90°, 120°, and 150° to investigate the effect of joint cross-angle on the damage evolution characteristics of rocks. In Figure 2(b), the joint cross-angle β is fixed as 100°, but the length LB of joint B is varied. The length LB of joint B is taken as 10 mm, 20 mm, 30 mm, 40 mm, and 50 mm to investigate the effect of joint length on the damage evolution characteristics of rocks.

2.2.2. Model Parameters. Since the PFC model reflects the macroscopic mechanics of rock by the mechanical properties of particles and the interparticle contact and these parameters cannot be obtained directly from the indoor experiments, the parameters of the model need to be calibrated before the numerical simulation. Typically, the parameters used by the PBM can be obtained from uniaxial compression tests [30]. The specific methods are as follows: firstly, a PBM with the same scale as the indoor uniaxial compression test model is established; secondly, the same mechanical loading scheme as the indoor experiments is used to obtain the mechanical properties of the numerical model; finally, the meso-parameters of the PBM are repeatedly calibrated by the "trial-and-error" method until the macroscopic parameters (e.g., elastic modulus and uniaxial compressive strength) and damage modes of the PBM are consistent with or similar to those of the indoor experiments. The final determined parameters can then be used for the analysis of different numerical schemes.

Due to the lack of indoor experimental data, the numerical parameters calibrated by Chen et al. [14] were used to establish the numerical models. The rock used in the research conducted by Chen et al. [14] was green sandstone, and the density, modulus of elasticity, and UCS of the rock were 2500 kg/m^3, 13.73 GPa, and 81.4 MPa, respectively. The deviation of E and UCS between the indoor experiment and the PFC numerical model is 0.39 GPa and 0.34 MPa.

The meso-parameters of the numerical green sandstone model calibrated by the "trial-and-error" method are shown in Table 1. The stress-strain curves and damage modes of the numerical model obtained by the uniaxial compression test based on meso-parameters are shown in Figures 3 and 4. As can be seen from the figures, the test results of the numerical model are in good agreement with the experimental results, so the meso-parameters in Table 1 can be used to build the PBM required in this paper.

Due to the difficulty of obtaining the mechanical and geometric parameters of actual joints, the bond properties of joints are set to 5% of the bond properties of particles (intact rock) by using the experience of Wang et al. [31], and the mechanical properties of joints in different parts of rock mass are assumed to be the same. The meso-parameters of joints are also obtained by referring to the study conducted by Chen et al. [14], and the specific parameters are shown in Table 2.

2.3. AE Simulation Based on PFC. When the force on the PBM as well as the SJM is greater than its bond strength (i.e., tensile strength or shear strength), the bond between the particles breaks, which corresponds to the creation of microcracks in the rock [32]. In general, during rock crack extension, damage energy will be rapidly released in the form of acoustic waves, which is the so-called acoustic emission phenomenon. Therefore, we can write FISH language to monitor the number of particle bond fractures during rock damage in real time and then analyze the acoustic emission characteristics during rock damage by counting the number of bond fractures at each moment (time step).

2.4. Loading Condition. This paper mainly investigates the mechanical properties, acoustic emission characteristics, and damage evolution law of rock models containing different cross-joints under uniaxial compression conditions, so the loading method in this paper is the same as the indoor uniaxial compression loading. In general, there are two modes of uniaxial compression experiments, displacement loading and stress loading, and this paper adopts the displacement loading mode. In order to improve the running efficiency, a loading speed of 0.001 m/s is adopted by moving the wall on top of the model. Although this loading speed is higher than that of general indoor experiments, many studies show that when the loading speed of PFC model is

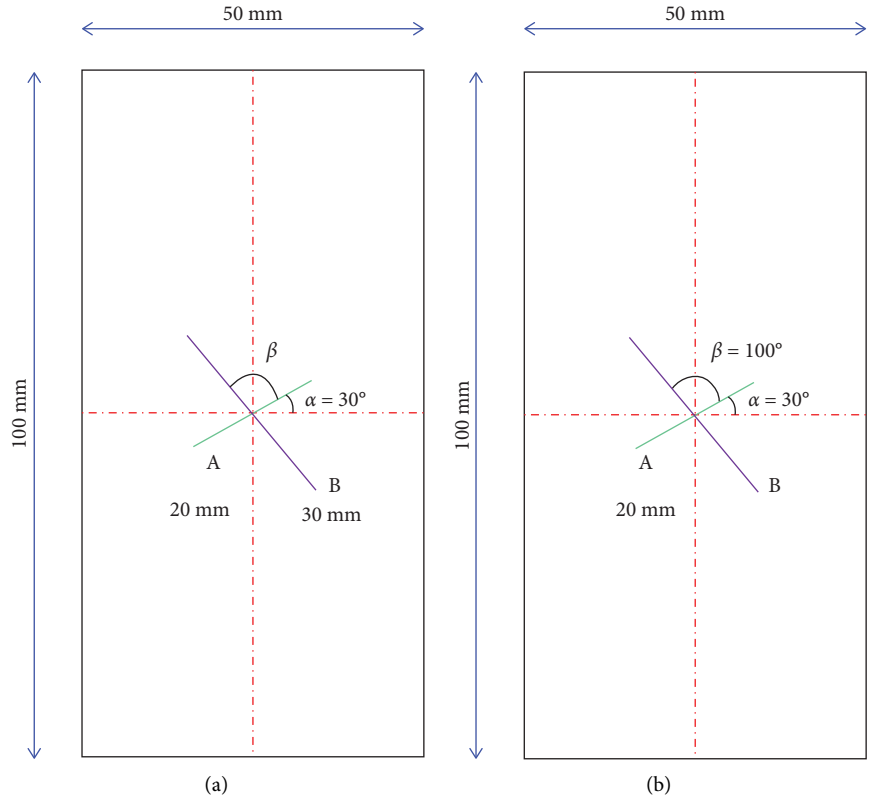

Figure 2: Schemes of rock models with a set of cross-joints with different (a) joint cross-angles and (b) joint lengths.

Table 1: Meso-parameters for the PBM [14].

Parameter	Value
Minimum particle diameter (mm)	0.3
Maximum particle diameter (mm)	0.5
Contact modulus of the particle (GPa)	10
Parallel bond deformation modulus (GPa)	16
Contact bond gap (mm)	0.05
Porosity	0.1
Density (kg/m^3)	2500
Parallel bond tensile strength (MPa)	21.7
Parallel bond cohesive force (MPa)	56
Stiffness ratio	1.5

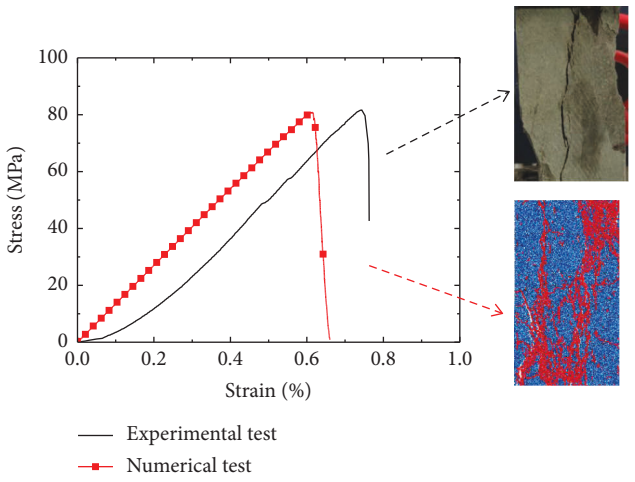

Figure 3: Comparison of experimental and numerical results of stress-strain curves and damage modes [14].

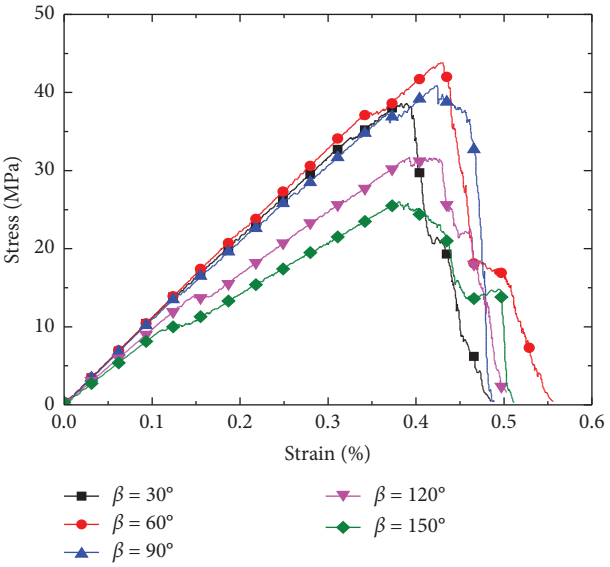

Figure 4: Stress-strain curves of rocks with different joint cross-angles.

Table 2: Meso-parameters for the SJM [11].

Parameter	Value
Joint tensile strength (MPa)	1.085
Joint cohesive force (MPa)	2.8
Joint friction angle	30
Joint normal stiffness (GPa/m)	15
Joint tangential stiffness (GPa/m)	10
Joint width (mm)	1

less than 0.1 m/s, the difference of axial stress-axial strain curve and strength parameters between numerical specimens is very small [33, 34].

3. Mechanical Properties and AE Evolution Characteristics of Different Rock Models

3.1. Mechanical Properties

3.1.1. Effect of Joint Cross-Angle. Figures 4 and 5 show the stress-strain curves as well as the uniaxial compressive strength and elastic modulus of rocks with different joint cross-angles, respectively. From the figures, it can be seen that the UCS and E of jointed rocks show a trend of increase and then decrease with the increase of joint cross-angle β. As the joint cross-angle β increases from 30° to 150°, the UCS of jointed rocks is 38.64 MPa, 43.85 MPa, 40.91 MPa, 31.74 MPa, and 26.02 MPa and the E is 11.21 GPa, 11.24 GPa, 10.96 GPa, 9.51 GPa, and 8.59 GPa, respectively. The UCS and E of jointed rocks are highest when the joint cross-angle β is 60°. The main reason is that when the cross-angle β is 60°, the dip angle of joint B with the horizontal direction (i.e., $\alpha + \beta$) is 90°, while many studies have shown that a 90° dip angle of joints has less effect on the mechanical properties of rocks [35].

3.1.2. Effect of Joint Length. Figures 6 and 7 show the stress-strain curves as well as the uniaxial compressive strength and elastic modulus of rocks with different joint lengths (the length of joint B, LB), respectively. From the figures, it can be seen that the UCS and E of jointed rocks show a trend of decrease with the increase of joint length. As the joint length increases from 10 mm to 50 mm, the UCS of jointed rocks is 42.41 MPa, 41.87 MPa, 37.18 MPa, 36.89 MPa, and 21.39 MPa and the E is 11.58 GPa, 11.31 GPa, 10.52 GPa, 9.22 GPa, and 7.09 GPa, respectively. The main reason is that as the length of joints increases, the penetration of joints increases and the extent of weak structure throughout the rock becomes larger, which in turn leads to a decrease in the mechanical properties of the jointed rock.

3.2. AE Evolution Characteristics

3.2.1. Effect of Joint Cross-Angle. Figure 8 shows the acoustic emission evolution characteristic curves of rocks containing different joint cross-angles. From the figure, it can be seen that, with the increasing load loading time, the stress in the jointed rock shows a characteristic of fluctuating increase until the peak and then fluctuating decrease. Along with the evolution of stress, the acoustic emission counts of jointed rocks show three stages. The first stage is the stage of linear rise of the stress curve. At this time, no cracks are produced inside the jointed rocks, and the number of acoustic emission counts from the jointed rocks is zero. This stage can be called the acoustic emission-free stage. The second stage is the stage of rising fluctuation of stress curve. At this time, the cracks inside the jointed rocks are gradually developed, and the acoustic emission counts are jumping, i.e., there are

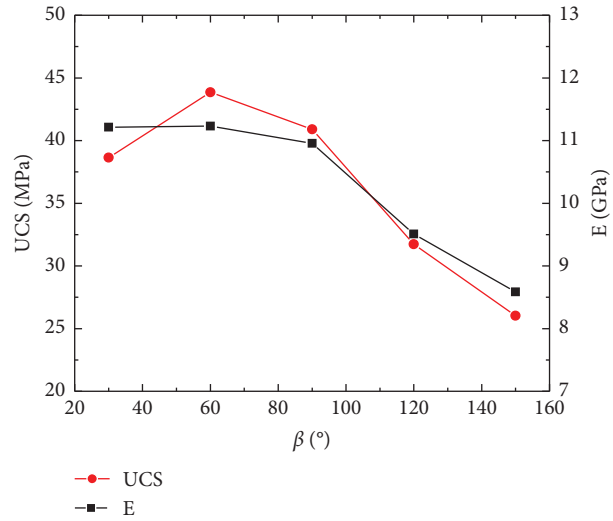

Figure 5: UCS and E of rocks with different joint cross-angles.

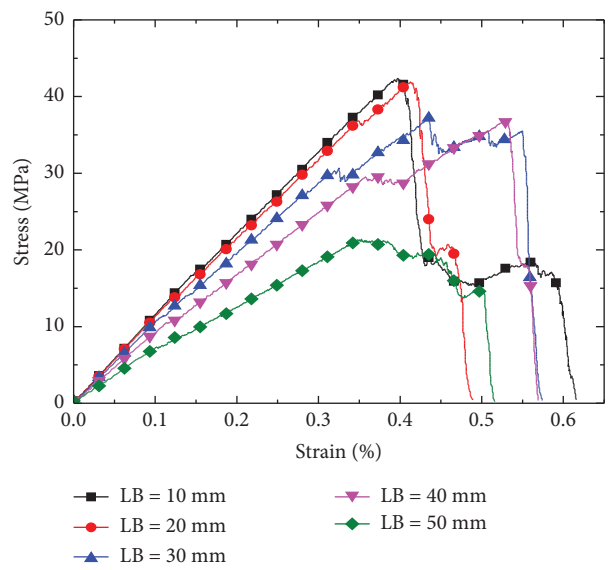

Figure 6: Stress-strain curves of rocks with different joint lengths.

moments of sudden increase, while others are not, which is related to the damage characteristics inside the jointed rocks. Overall, the increase in acoustic emission intensity (the number of acoustic emission counts at the same time step) in this phase is not very large and can be called the phase of slow increase of acoustic emission. The third stage is around the peak of the stress curve. At this time, the cracks inside the jointed rocks increase sharply, and the acoustic emission counts also jump, but the intensity of acoustic emission is much larger than that of the second stage. Therefore, the third stage can be called the stage of sharply increasing acoustic emission.

In addition, it can also be seen from Figure 8 that the overall trend of the acoustic emission evolution of jointed rocks does not change with the change of joint cross-angle. However, the time step of the occurrence of acoustic emission (crack initiation time) has changed. As the joint

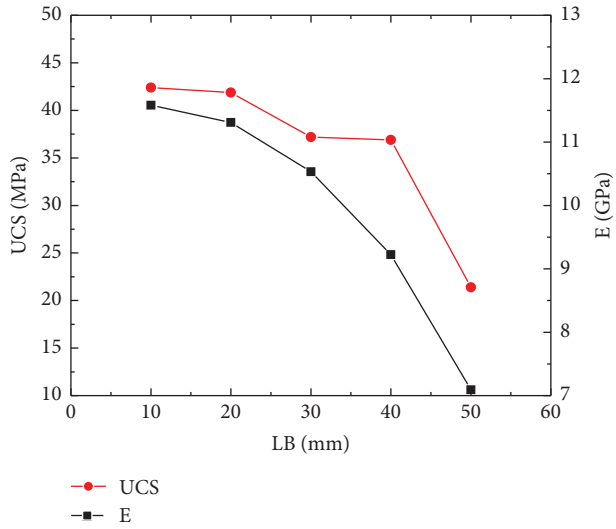

Figure 7: UCS and E of rocks with different joint lengths.

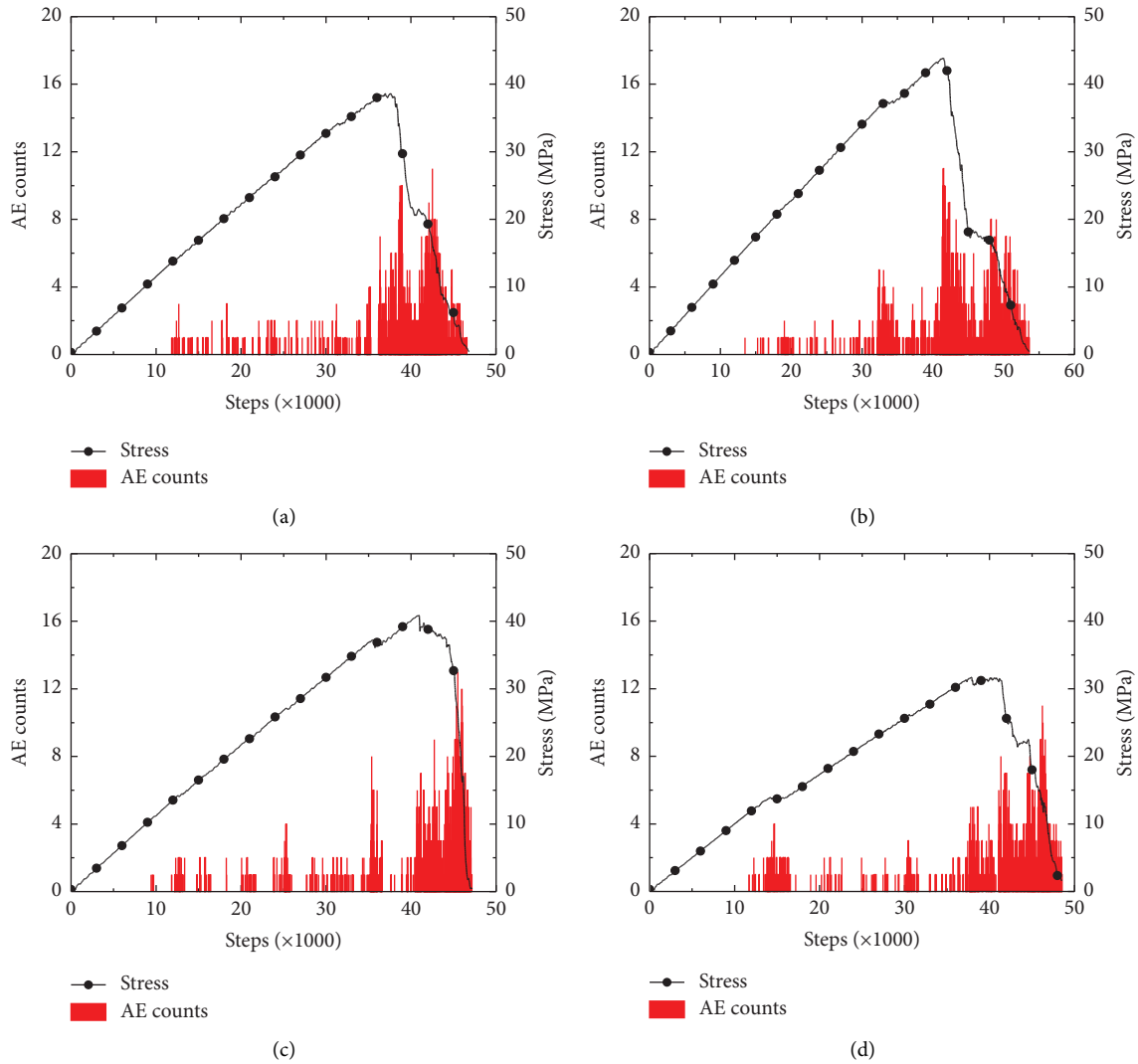

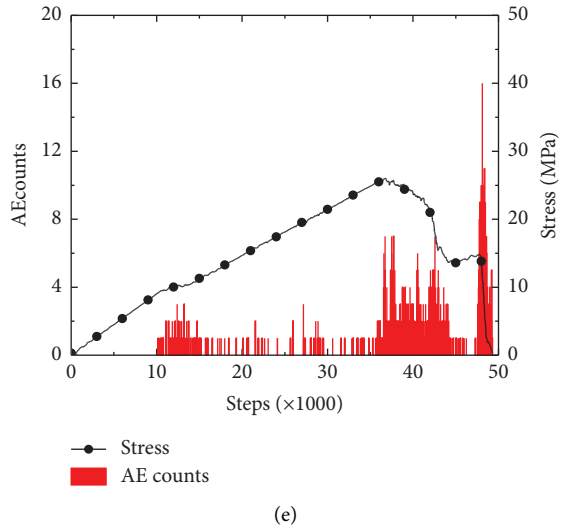

Figure 8: AE counts of rocks with different joint cross-angles. (a) $\beta = 30^{\circ}$. (b) $\beta = 60^{\circ}$. (c) $\beta = 90^{\circ}$. (d) $\beta = 120^{\circ}$. (e) $\beta = 150^{\circ}$.

cross-angle β increases from 30° to 150°, the time step of the occurrence of acoustic emission is 11776, 15321, 9598, 11582, and 10100, respectively. The largest time step of the occurrence of acoustic emission is for the rock with β equal to 60°, and the UCS and E of this jointed rock are the largest. Overall, the better the mechanical properties of the jointed rock, the less likely it is that internal cracks will form and the acoustic emission will be generated later. Besides, the maximum value of AE counts and the time of its occurrence vary with the variation of joint cross-angle β. As the joint cross-angle β increases from 30° to 150°, the maximum values of acoustic emission counts of jointed rocks are 11, 10, 13, 10, and 11, showing a "W"-type trend, and the time corresponding to the maximum values of acoustic emission counts is 42510, 41409, 45576, 46363, and 48347. Overall, the maximum value of acoustic emission and the occurrence time step have few relationships with the change of joint cross-angle β, and the relationship with UCS and E is also not obvious. Nevertheless, the evolution characteristics of acoustic emission changes are more closely related to the fluctuation characteristics of stress, and the time step of the acoustic emission jump is consistent with the time step of the stress fluctuation.

3.2.2. Effect of Joint Length. Figure 9 shows the characteristic curves of acoustic emission evolution of rocks with different joint lengths. As can be seen from the figure, the overall trend of the evolution of acoustic emission of jointed rocks does not change greatly as the length of joint B changes, and they all go through three stages: no acoustic emission, slowly increasing acoustic emission, and sharply increasing acoustic emission. However, with the increase of joint length, the phase of sharp increase of acoustic emission changes from two to one. Besides, the overall trend of the time step of the occurrence of acoustic emission decreases with the increase of joint length. As the joint length LB increases from 10 mm to 50 mm, the time step of the occurrence of acoustic emission is 11589, 9507, 9853, 8563, and 7411, respectively. The largest time step of the occurrence of acoustic emission is for the rock with LB equal to 10 mm, and the UCS and E of this jointed rock are the largest. Overall, the shorter the joint length of the rock (the smaller the penetration), the better its mechanical properties, the less likely its internal cracks will form, and the later the generation of acoustic emission. In addition, the maximum value of acoustic emission counts and the time of its occurrence vary with the variation of joint length. As the joint length LB increases from 10 mm to 50 mm, the maximum values of acoustic emission of jointed rocks are 10, 20, 16, 16, and 11, showing a trend of increase and then decrease, and the time corresponding to the maximum values of acoustic emission is 54878, 41028, 53734, 51846, and 48717. Overall, the maximum value of acoustic emission and its time step of occurrence are not obvious in relation to the variation of joint length and are not obvious in relation to UCS and E.

4. Damage Evolution of Different Rock Models Based on AE Characteristics

4.1. Damage Variables Based on AE Characteristics. The scholar Kachanov [36] of the former Soviet Union defined the damage variable as follows:

$$D = \frac{A_i}{A}, \tag{1}$$

where A_i is the damage cross-sectional area of the rock material in a certain period and A is the cross-sectional area of the material without damage at the initial stage.

If the cumulative acoustic emission count at the time when the nondestructive cross-sectional area A of the rock samples completely loses the bearing capacity is W, then the cumulative acoustic emission count W_u of the unit area of rock failure is

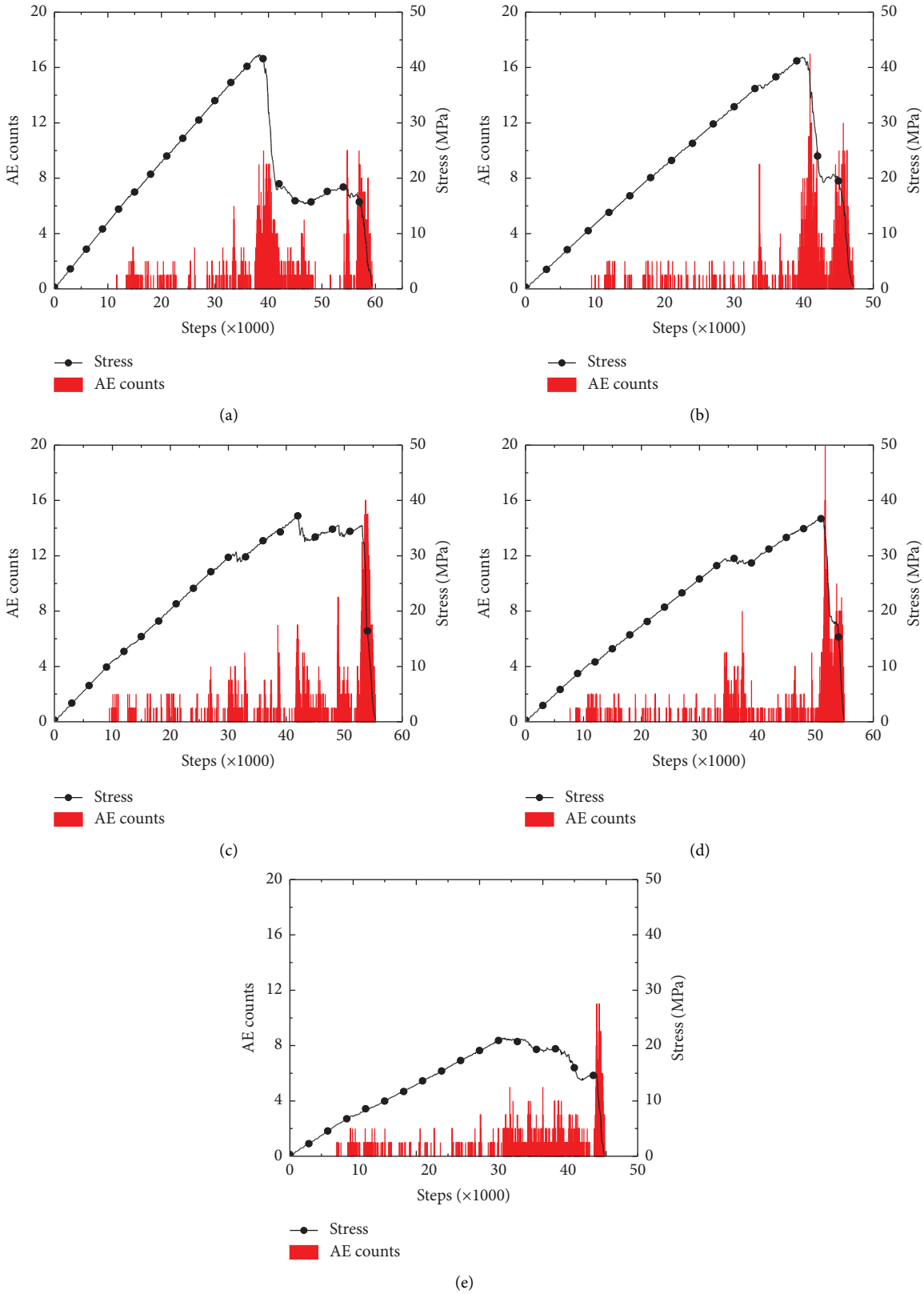

Figure 9: AE counts of rocks with different joint lengths. (a) LB = 10 mm. (b) LB = 20 mm. (c) LB = 30 mm. (d) LB = 40 mm. (e) LB = 50 mm.

$$W_u = \frac{W}{A}. \quad (2)$$

When the damage cross-sectional area of the rock samples reaches A_i, the number of cumulative acoustic emission counts W_t can be calculated as

$$W_t = W_u \cdot A_i = \frac{W}{A} \cdot A_i. \quad (3)$$

Thus,

$$D = \frac{A_i}{A} = \frac{W_t}{W}. \quad (4)$$

Many studies [3, 14] have shown that the damage variables using (4) can better respond to the damage characteristics of rocks, so we next explore the damage evolution patterns of different jointed rocks by using the damage variables defined by (4).

4.2. Damage Evolution of Different Jointed Rock Models

4.2.1. Effect of Joint Cross-Angle. Figure 10 shows the damage evolution characteristics of rocks with different joint cross-angles. From the figure, it can be seen that the damage evolution of jointed rocks shows three stages with the increase of stress (time). The first stage is the damage-free stage, which corresponds to the no acoustic emission stage in acoustic emission evolution characteristic curves. At this time, no cracks are produced inside the jointed rock, which mainly corresponds to points a ~ b in the figure. The second stage is the slow (fluctuating) increasing stage of damage, which corresponds to the slow increasing stage of acoustic emission evolution characteristics. Within this phase, cracks within the rock are continuously developed and acoustic emission occurs in jumps, which mainly corresponds to points b ~ d in the figure. The third stage is the stage of sharp increase of damage, which corresponds to the sharp increase of acoustic emission evolution characteristics. In this stage, the rock internal cracks develop rapidly and the acoustic emission signal is more intense, mainly corresponding to points d ~ f in the figure.

From Figure 10, we also know that the trend of damage evolution characteristics of jointed rocks does not change with the increase of joint cross-angle, and all go through three damage characteristic stages. However, the fluctuation characteristics during the damage evolution of jointed rocks are different with the change of joint cross-angle. When the joint cross-angle β is 30°, the slow increasing phase of jointed rock damage is relatively gentle, and the sharp increasing phase of damage is relatively steep and less fluctuating. When the joint cross-angle β is 60°~120°, the slow increasing stage of the jointed rock damage shows two steps, the sharp increasing stage of damage also shows two steps, and the slope of the first step has the tendency to become larger with the increase of β. Overall, the damage evolution trend of jointed rocks is related to the stress characteristics, and the fluctuation of damage is also due to the fluctuation generated by stress. Therefore, the damage variables defined by using acoustic emission can better reflect the damage evolution characteristics of jointed rocks.

Figure 11 shows the damage evolution of rocks with different joint cross-angles. From the figure, it can be seen that the damage rupture of jointed rocks begins to sprout from and expand along the tip of the joints. In points a ~ c, cracks are mainly produced at the tips of the joints. When entering point d, the cracks develop continuously around the two joints. When entering points e ~ f, the development of cracks is more extensive and begins to spread throughout the model until the model is destroyed.

For rocks with different joint cross-angles, the damage rupture process during loading is different. When the joint angle is 30°~90°, the initial damage of the jointed rock is mainly at the tip of joint B, followed by cracks near joints A and B, and finally the damage block is formed on the left side of the jointed rock and detached from the rock. Of course, for the rock with a joint angle of 60°, the right side of the rock masses also formed a destruction block. When the joint angle is 120°, the initial damage of the jointed rock is at the right-hand tips of joints A and B, which then extends to the left-hand tips of the joints and finally forms larger cracks in the upper part of the jointed rock, thus leading to rock destruction. For a jointed rock with a joint angle of 150°, the initial damage is at the tip of joint A, then extends to the tip of joint B, and finally continues to extend along the tip of joint B until the rock breaks down.

4.2.2. Effect of Joint Length. Figure 12 shows the damage evolution characteristics of rocks with different joint lengths. From the figure, we can know that the trend of damage evolution characteristics of rocks does not change with the increase of the length of joints, and they all go through three characteristic stages as described in Section 3.2.1. However, the fluctuation characteristics of the damage evolution of jointed rocks are different with the variation of joint length. When the length of the joint is 10 mm, the slow damage phase of the rock is between point b and point c, with a small increase, and the sharp increase phase of the rock is between point c and point f, with a large increase and the existence of two steps. When the length of the joint is 20 mm, the slow damage phase of the rock is between point b and point d, with a small increase; the sharp increase phase of the rock is between point d and point f, with a larger increase; and the stage phase is small. When the length of joints is 30 mm, the slow damage phase of the rock is between point b and point c, the sharp increase phase of the rock is between point c and point f, and the increase rate in phase c~e is smaller than that in phase e ~ f. When the length of joints is 40 mm, the slow damage stage of the rock is between point b and point c; the sharp increase stage of the damage of the rock is between point c and point f; and there are two steps. The increase rate in the first step is slower than that in the second step. When the length of the joint is 50 mm, the slow damage phase of the rock is between point b and point c, the sharp increase phase of the rock is between point c and point f, and the increase rate in phase c to e is balanced and less than the sharp increase in phase e to f.

Figure 13 shows the damage evolution of rocks with different joint lengths. It can be seen from the figure the damage evolution process of jointed rocks shows some

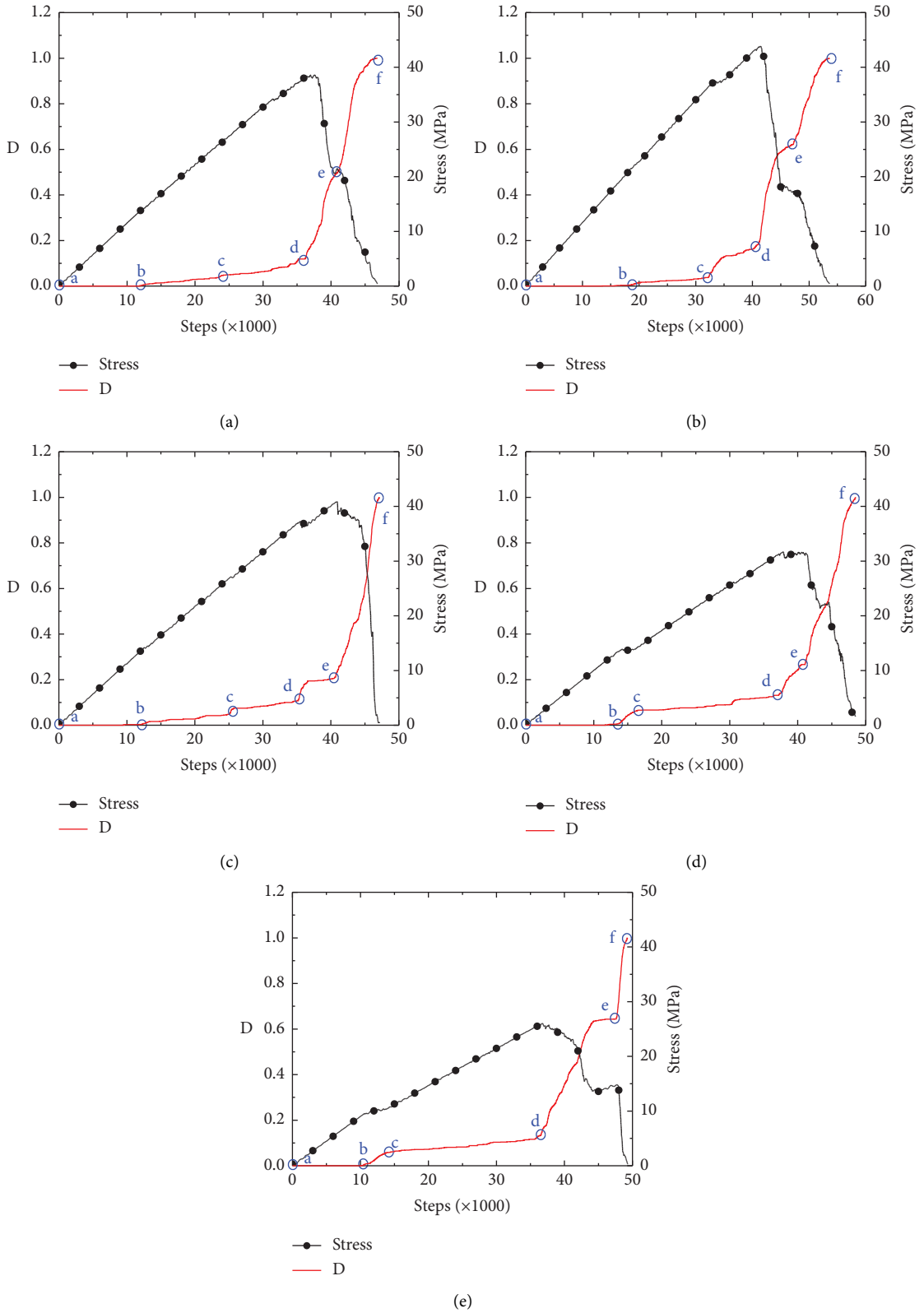

Figure 10: Damage evolution characteristics of rocks with different joint cross-angles. (a) $\beta = 30^{\circ}$. (b) $\beta = 60^{\circ}$. (c) $\beta = 90^{\circ}$. (d) $\beta = 120^{\circ}$. (e) $\beta = 150^{\circ}$.

Rock models With different β	Key point					
	a	b	c	d	e	f
$\beta = 30°$		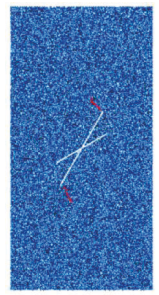	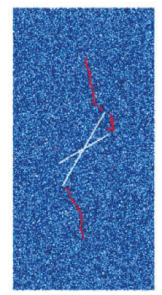	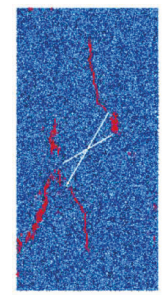	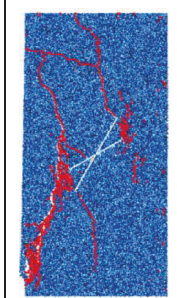	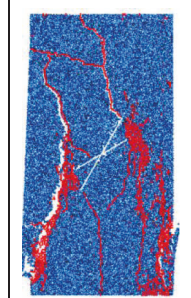
$\beta = 60°$	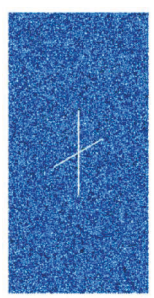	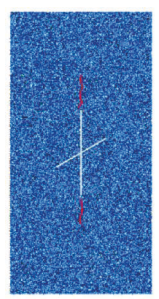	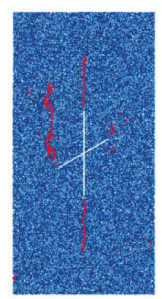	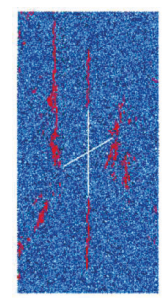	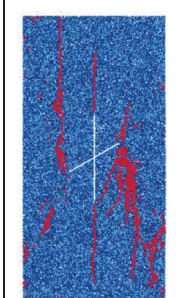	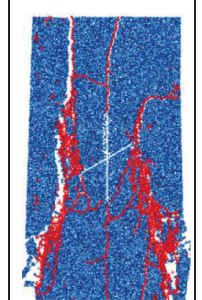
$\beta = 90°$	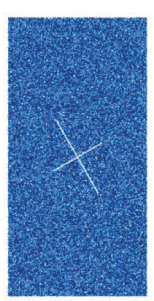	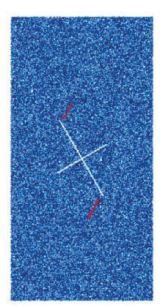	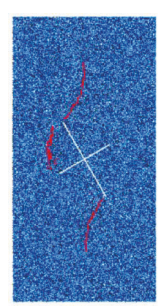	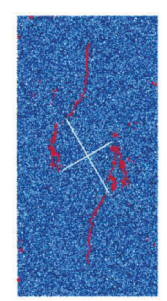	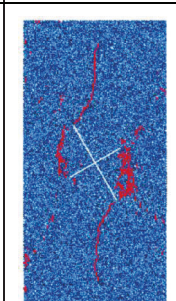	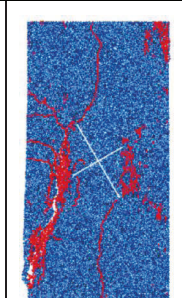
$\beta = 120°$	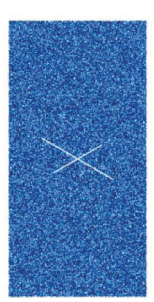	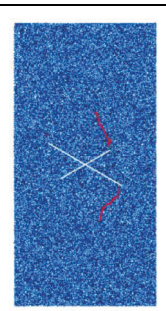	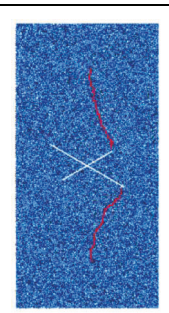	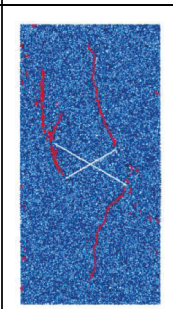	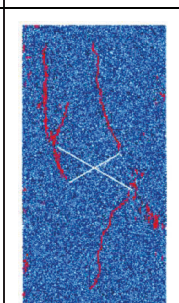	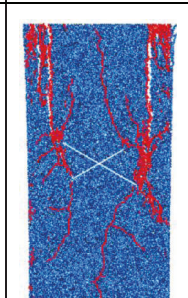
$\beta = 150°$	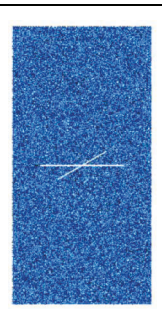	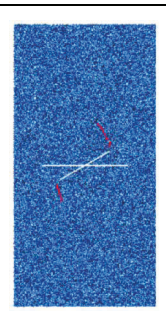	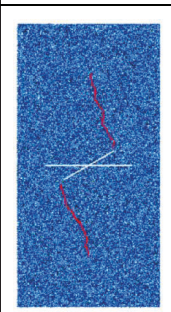	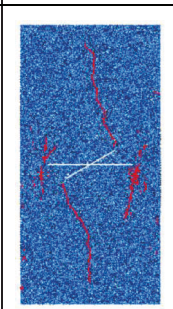	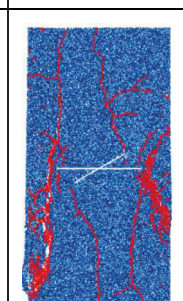	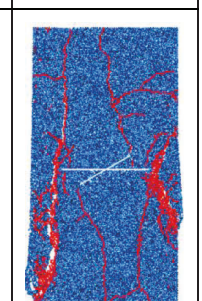

Figure 11: Damage evolution of rocks with different joint cross-angles.

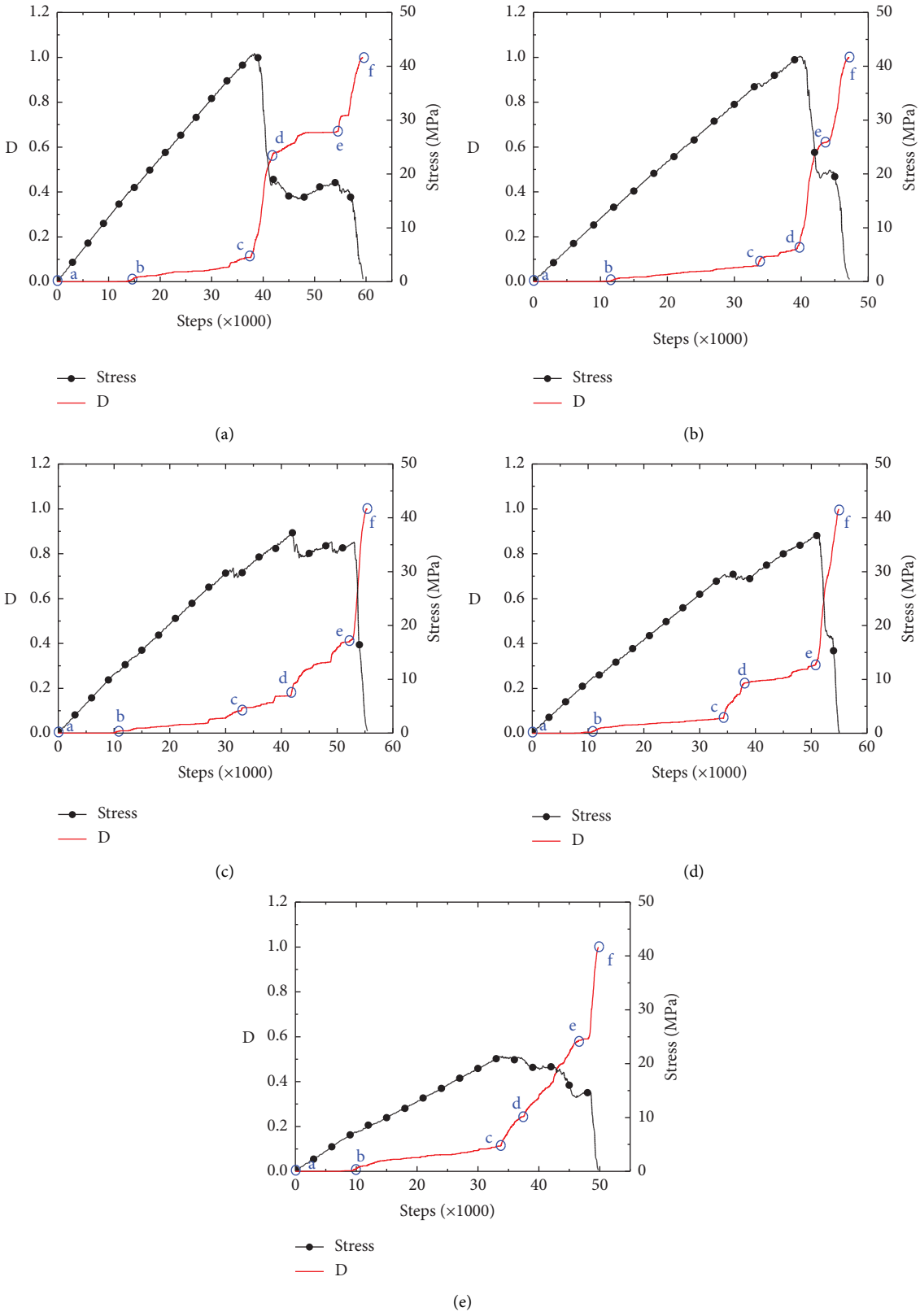

Figure 12: Damage evolution characteristics of rocks with different joint lengths. (a) LB = 10 mm. (b) LB = 20 mm. (c) LB = 30 mm. (d) LB = 40 mm. (e) LB = 50 mm.

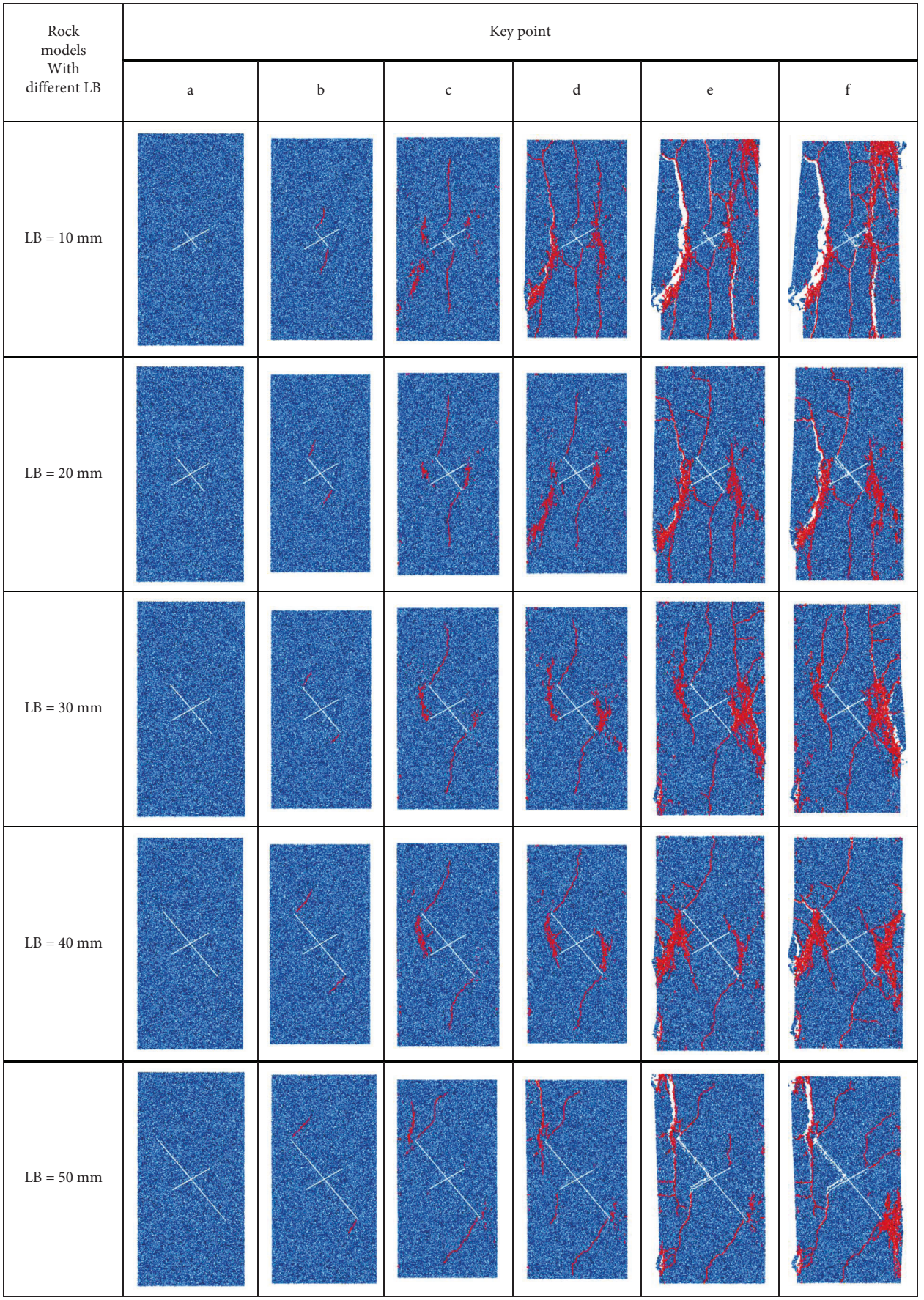

Figure 13: Damage evolution of rocks with different joint lengths.

similarity with the different lengths of joints, mainly in the crack budding stage and the slow development stage. In the crack initiation stage, the cracks are first produced at the tips of joint B. Subsequently, cracks along joint B are continuously expanded and mixed with cracks in joint A. However, the final damage state of jointed rocks varies with the length of joints. When the length of joints is small, the splitting block of the rock is larger and the cracks extend closer to the center of the rock. When the length of joints is large, the damage of the rock gradually breaks towards the edge of the rock, such as the upper left corner and the lower right corner.

5. Conclusions

This paper numerically investigates the effects of joint angle and joint length on the mechanical properties, acoustic emission characteristics, and damage evolution characteristics of jointed rocks based on particle flow code, and the following conclusions are obtained.

The UCS and E of jointed rocks show a trend of increase and then decrease with the increase of joint cross-angle β. The UCS and E of the jointed rock are highest when the joint cross-angle β is 60°. The UCS and E of jointed rocks show a trend of decrease with the increase of joint length.

Along with the evolution of stress, the acoustic emission counts of jointed rocks show three stages: acoustic emission-free stage, slow AE increase stage, and sharp AE increase stage. The overall trend of the AE evolution of jointed rocks does not change with the change of joint cross-angle and joint length. However, the time step of the occurrence of acoustic emission (crack initiation time) has changed. Overall, the better the mechanical properties of the jointed rock, the later the acoustic emission will be generated. The maximum value of AE and the occurrence time step have few relationships with the change of β and LB, and the relationship with UCS and E is also not obvious.

The damage evolution of jointed rocks shows three stages with the increase of stress (time): damage-free stage, slow damage increase stage, and sharp damage increase stage. The trend of damage evolution characteristics of jointed rocks does not change with the increase of joint cross-angle or joint length, and all go through three damage characteristic stages. However, the fluctuation characteristics of the damage evolution of jointed rocks are different with the change of β and LB.

The damage variables defined by using acoustic emission can better reflect the damage evolution characteristics of jointed rocks. The damage rupture of jointed rocks begins to sprout from and expand along the tip of the joints. The damage rupture of jointed rocks is different with the change of β and LB, which is mainly reflected in the crack initiation position and the final failure mode. For rocks with different β, the crack initiation position and the final failure mode are different; however, for rocks with different LB, the crack initiation position is similar.

Data Availability

The data used to support the findings of this study are included in the article.

Conflicts of Interest

The authors declare that they have no conflicts of interest.

Acknowledgments

This research was funded by the National Natural Science Foundation of China (52109139 and 52009122), the China Postdoctoral Science Foundation (2022M712724), the Natural Science Foundation of Zhejiang Province (LQ20E080022 and LQ21E090002), and the Science and Technology Project supported by the Department of Transportation of Zhejiang Province (2019007).

References

[1] D. Mas Ivars, M. E. Pierce, C. Darcel et al., "The synthetic rock mass approach for jointed rock mass modelling," *International Journal of Rock Mechanics and Mining Sciences*, vol. 48, no. 2, pp. 219–244, 2011.

[2] F. Ren, C. Zhu, and M. He, "Moment tensor analysis of acoustic emissions for cracking mechanisms during schist strain burst," *Rock Mechanics and Rock Engineering*, vol. 53, no. 1, pp. 153–170, 2020.

[3] W. Liu, J. Xu, Z. Wang, and C. Peng, "Experimental research on damage characteristics and safety damage threshold of jointed caverns based on acoustic emissions," *Geomechanics and Geophysics for Geo-Energy and Geo-Resources*, vol. 7, no. 3, pp. 72–14, 2021.

[4] Y. Wang, W. H. Tan, D. Q. Liu, Z. Q. Hou, and C. H. Li, "On anisotropic fracture evolution and energy mechanism during marble failure under uniaxial deformation," *Rock Mechanics and Rock Engineering*, vol. 52, no. 10, pp. 3567–3583, 2019.

[5] M. C. He, Q. R. Sui, M. N. Li, Z. J. Wang, and Z. G. Tao, "Compensation excavation method control for large deformation disaster of mountain soft rock tunnel," *International Journal of Mining Science and Technology*, 2022.

[6] G. Feng, X. C. Wang, Y. Kang, and Z. T. Zhang, "Effect of thermal cycling-dependent cracks on physical and mechanical properties of granite for enhanced geothermal system," *International Journal of Rock Mechanics and Mining Sciences*, vol. 134, Article ID 104476, 2020.

[7] R. H. Cao, P. Cao, H. Lin, X. Fan, C. Zhang, and T. Liu, "Crack initiation, propagation, and failure characteristics of jointed rock or rock-like specimens: a review," *Advances in Civil Engineering*, vol. 201931 pages, Article ID 6975751, 2019.

[8] H. Lee and S. Jeon, "An experimental and numerical study of fracture coalescence in pre-cracked specimens under uniaxial compression," *International Journal of Solids and Structures*, vol. 48, no. 6, pp. 979–999, 2011.

[9] P. Yin, R. H. C. Wong, and K. T. Chau, "Coalescence of two parallel pre-existing surface cracks in granite," *International Journal of Rock Mechanics and Mining Sciences*, vol. 68, pp. 66–84, 2014.

[10] S. Q. Yang, "Crack coalescence behavior of brittle sandstone samples containing two coplanar fissures in the process of deformation failure," *Engineering Fracture Mechanics*, vol. 78, no. 17, pp. 3059–3081, 2011.

[11] X. P. Zhou, H. Cheng, and Y. F. Feng, "A "n experimental study of crack coalescence behaviour in rock-like materials containing multiple flaws under uniaxial compression"," *Rock Mechanics and Rock Engineering*, vol. 47, no. 6, pp. 1961–1986, 2014.

[12] H. Li and L. N. Y. Wong, "Influence of flaw inclination angle and loading condition on crack initiation and propagation," *International Journal of Solids and Structures*, vol. 49, no. 18, pp. 2482–2499, 2012.

[13] X. P. Zhang and L. N. Y. Wong, "Cracking processes in rock-like material containing a single flaw under uniaxial compression: a numerical study based on parallel bonded-particle model approach," *Rock Mechanics and Rock Engineering*, vol. 45, no. 5, pp. 711–737, 2012.

[14] Z. Chen, L. Xu, and Y. Shang, "Influence of joint angle on the acoustic emission evolution characteristics and energy dissipation rule of rock mass," *Geotechnical & Geological Engineering*, vol. 39, no. 2, pp. 1621–1635, 2021.

[15] M. R. Vergara, M. Van Sint Jan, and L. Lorig, "Numerical model for the study of the strength and failure modes of rock containing non-persistent joints," *Rock Mechanics and Rock Engineering*, vol. 49, no. 4, pp. 1211–1226, 2016.

[16] V. Sarfarazi, R. K. zadeh, K. Asgari, and X. Wang, "H" shaped echelon joints under uniaxial loading," *Geotechnical & Geological Engineering*, vol. 40, no. 4, pp. 1765–1787, 2022.

[17] Z. A. Moradian, G. Ballivy, P. Rivard, C. Gravel, and B. Rousseau, "Evaluating damage during shear tests of rock joints using acoustic emissions," *International Journal of Rock Mechanics and Mining Sciences*, vol. 47, no. 4, pp. 590–598, 2010.

[18] J. F. Hazzard and R. P. Young, "Simulating acoustic emissions in bonded-particle models of rock," *International Journal of Rock Mechanics and Mining Sciences*, vol. 37, no. 5, pp. 867–872, 2000.

[19] C. Khazaei, J. Hazzard, and R. Chalaturnyk, "Damage quantification of intact rocks using acoustic emission energies recorded during uniaxial compression test and discrete element modeling," *Computers and Geotechnics*, vol. 67, pp. 94–102, 2015.

[20] Q. B. Lin, P. Cao, K. H. Li, R. H. Cao, K. P. Zhou, and H. W. Deng, "Experimental study on acoustic emission characteristics of jointed rock mass by double disc cutter," *Journal of Central South University*, vol. 25, no. 2, pp. 357–367, 2018.

[21] Z. Chong, Q. Yao, X. Li, and K. Shivakumar, "Acoustic emission investigation on scale effect and anisotropy of jointed rock mass by the discrete element method," *Arabian Journal of Geosciences*, vol. 13, no. 9, pp. 324–414, 2020.

[22] Z. Zhang, X. Liu, Y. Zhang, X. Qin, and M. Khan, "Comparative study on fracture characteristics of coal and rock samples based on acoustic emission technology," *Theoretical and Applied Fracture Mechanics*, vol. 111, Article ID 102851, 2021.

[23] W. Liu, W. Yuan, Y. Yan, and X. Wang, "Analysis of acoustic emission characteristics and damage constitutive model of coal-rock combined body based on particle flow code," *Symmetry*, vol. 11, no. 8, p. 1040, 2019.

[24] P. Zhang, Y. He, Z. Sun, and D. Yue, "Influence of parallel-joint position on mechanical behavior and acoustic emission characteristics of rock pillar," *Shock and Vibration*, vol. 2021, pp. 1–9, Article ID 1719553, 2021.

[25] J. Zhou, Y. Chi, Y. W. Chi, and J. P. Xu, "The method of particle flow and PFC2D Code," *Rock and Soil Mechanics*, vol. 21, no. 3, pp. 271–274, 2000.

[26] Itasca Consulting Group Inc, *PFC (Particle Flow Code), version 5.0*, ICG, Minnesota, MN, USA, 2014.

[27] M. Chen, S. Q. Yang, P. G. Ranjith, and Y. C. Zhang, "Cracking behavior of rock containing non-persistent joints with various joints inclinations," *Theoretical and Applied Fracture Mechanics*, vol. 109, Article ID 102701, 2020.

[28] S. Wu and X. Xu, "A study of three intrinsic problems of the classic discrete element method using flat-joint model," *Rock Mechanics and Rock Engineering*, vol. 49, no. 5, pp. 1813–1830, 2016.

[29] M. Bahaaddini, A. M. Sheikhpourkhani, and H. Mansouri, "Flat-joint model to reproduce the mechanical behaviour of intact rocks," *European Journal of Environmental and Civil Engineering*, vol. 25, no. 8, pp. 1427–1448, 2021.

[30] U. Castro-Filgueira, L. R. Alejano, J. Arzúa, and D. M. Ivars, "Sensitivity analysis of the micro-parameters used in a PFC analysis towards the mechanical properties of rocks," *Procedia Engineering*, vol. 191, pp. 488–495, 2017.

[31] P. Wang, M. Cai, F. Ren, C. Li, and T. Yang, "A digital image-based discrete fracture network model and its numerical investigation of direct shear tests," *Rock Mechanics and Rock Engineering*, vol. 50, no. 7, pp. 1801–1816, 2017.

[32] J. F. Hazzard, R. P. Young, and S. C. Maxwell, "Micro-mechanical modeling of cracking and failure in brittle rocks," *Journal of Geophysical Research: Solid Earth*, vol. 105, no. B7, pp. 16683–16697, 2000.

[33] P. Cheng, "Loading rate effect analysis on rock particle flow mode under uniaxial compression," *Chinese Journal of Underground Space and Engineering*, vol. 14, no. 3, pp. 635–642, 2017.

[34] X. p. Zhang, Q. Zhang, and S. Wu, "Acoustic emission characteristics of the rock-like material containing a single flaw under different compressive loading rates," *Computers and Geotechnics*, vol. 83, pp. 83–97, 2017.

[35] C. Huang, W. Yang, K. Duan, L. Fang, L. Wang, and C. Bo, "Mechanical behaviors of the brittle rock-like specimens with multi-non-persistent joints under uniaxial compression," *Construction and Building Materials*, vol. 220, pp. 426–443, 2019.

[36] L. M. Kachanov, "Rupture time under creep conditions," *International Journal of Fracture*, vol. 97, no. 1/4, pp. 11–18, 1999.